JOURNAL OF APPLIED PHYSICS **114**, 224502 (2013)

Deep-level traps induced dark currents in extended wavelength $In_xGa_{1-x}As$/InP photodetector

Xiaoli Ji,[1] Baiqing Liu,[1] Yue Xu,[1] Hengjing Tang,[2] Xue Li,[2] HaiMei Gong,[2] Bo Shen,[3] Xuelin Yang,[3] Ping Han,[1] and Feng Yan[1,a)]
[1]*School of Electronics Science and Engineering, Nanjing University, Nanjing 210093, China*
[2]*State Key Laboratory of Transducer Technology, Shanghai Institute of Technical Physics, Shanghai 200083, China*
[3]*Physics Department, Peking University, Beijing 100871, China*

(Received 19 October 2013; accepted 15 November 2013; published online 9 December 2013)

The dark current mechanism of extended wavelength $In_xGa_{1-x}As$ photo-detectors is still a debated issue. In this paper, the deep-level transient spectroscopy (DLTS) and dark current characteristics of $In_xGa_{1-x}As$/InP detectors are investigated. Using trap parameters obtained from DLTS measurement, the device simulations of current-voltage characteristics are carried out by Silvaco Altas. The results reveal that the dark current at the low reverse bias voltage is associated with deep level trap induced trap assisted tunneling and Shockley-Read-Hall generation mechanism. The reduction of the deep level trap concentration in $In_xGa_{1-x}As$ absorption layer could dramatically suppress the dark current near zero bias in extended wavelength $In_xGa_{1-x}As$/InP detectors. © *2013 AIP Publishing LLC*. [http://dx.doi.org/10.1063/1.4838041]

I. INTRODUCTION

The extended wavelength $In_xGa_{1-x}As$/InP photodetectors with x from 0.53 to 0.8 cover the short wavelength infrared (SWIR, 1.0–2.5 μm) range and have attracted much more attention due to their important applications in environmental research, earth observation, night vision, etc.[1–3] In such applications, the photo-detectors are operated at a bias voltage close to zero and subject to the temperature variation. It is advantageous for the detectors to have a low dark current over a wide temperature range. However currently, the extended wavelength $In_xGa_{1-x}As$/InP detectors suffer from the high dark current.[4,5] The increase of Indium composition (x) greater than 0.53 usually leads to the relatively high the lattice mismatch between $In_xGa_{1-x}As$ layer and InP substrate. The latter gives rise to the defects or traps densities in the forbidden gap, which can have important sequences for the dark current degradation. Even though the large lattice mismatch could be compensated by growing $InAs_yP_{1-y}$ or $In_yAl_{1-y}As$ buffer between the absorption and substrate layer,[6–8] the remains are still substantial (about 1%∼2%) for the electrical performance of the devices.[9]

The dark current mechanisms for extended wavelength $In_xGa_{1-x}As$ detectors are widely investigated from the temperature behavior of Current-voltage (I–V) curves. However, the different mechanisms have been reported by several groups. Li *et al.*[10] recently reported that near zero-bias dark current of $In_{0.78}Ga_{0.22}As$/InP detectors is contributed from the diffusion mechanism; Miao *et al.*[11] proposed that both diffusion and generation currents are the dominate dark current contributors in $In_{0.82}Ga_{0.18}As$/InP detectors while Hoogeveen *et al.*[12] reported that the dark currents in $In_xGa_{1-x}As$ (x = 0.81–0.83) devices are mainly associated with the generation-recombination and the tunneling mechanisms. In the latter case, it is proposed that the large dislocations in the absorption layer give rise to a distorted diffusion of the P-type doping, resulting in a locally higher electric field and the large tunneling current in $In_xGa_{1-x}As$ layer. These results evidence considerable progress in the understanding of the matter. However, to date the dark current mechanism for the extended wavelength $In_xGa_{1-x}As$ devices remain elusive.

For successfully realizing the dark current mechanism and further suppressing the dark current in extended wavelength $In_xGa_{1-x}As$ detectors, it is necessary to understand the properties of the defects or traps in the absorption layer. Deep-level transient spectroscopy (DLTS) could provide the important information of defect behaviors in the absorption layer.[13,14] Using the technique, the deep states in $In_{0.53}Ga_{0.47}As$/InP devices have been successfully determined[15–18] and they are reported to induce not only a dark generation current but a tunneling current.[19] In contrast to this, very little work has been conducted on the investigation of the trap behaviors for extended wavelength $In_xGa_{1-x}As$ detectors. Furthermore, to date no systematic studies of their influence on the dark current were reported for the detectors.

In this paper, we characterize I–V curves and the deep level traps in extended wavelength $In_xGa_{1-x}As$ (x = 0.78) on InP detectors. The response wavelength range of the detectors is between 1 μm and 2.4 μm. A deep level trap is observed. Using trap parameters obtained from DLTS measurement, a theoretical model of dark current is developed and the device simulations of I–V characteristic are carried out on the basis of this model by Silvaco Altas. It is found that the dark current near zero bias is strongly related to deep traps induced Shockley-Read-Hall generation and trap assisted tunneling mechanisms. Further reducing the deep level trap concentration in $In_xGa_{1-x}As$ absorption layer could dramatically suppress the dark current near zero bias in the detectors.

a)Email: fyan@nju.edu.cn. Tel.: +86-25-83593965. Fax: +86-25-83593965

II. EXPERIMENTAL

The devices used for the experiments is P^+ $InAs_yP_{1-y}$/$In_xGa_{1-x}As$/InP heterojunction structure detectors with ($x = 0.78$) produced by Judson company.[16] The structure is grown by metal-organic chemical vapor deposition (MOCVD) where the lattice mismatch between $In_xGa_{1-x}As$ and InP substrate is compensated by composition graded $InAs_yP_{1-y}$ buffer layers published elsewhere. The electrical measurements are conducted using Keithley 4200 semiconductor characterization system in Cascade Summit 12000 probe station with a built-in temperature controller. The temperature of sample holder can be tuned from 210 K to 470 K continuously with an error less than 0.1 K. The doping density in $In_xGa_{1-x}As$ layer is deduced from C–V measurements. DLTS measurements are conducted using DLS-83D Deep Level Transient Spectroscopy test system and analyzed using standard techniques. The test temperature of sample can be turned from 20 K to 300 K continuously. The device simulations for dark currents have been carried out by Silvaco Altas software.

III. RESULTS AND DISCUSSIONS

A. Deep-level transient spectroscopy and I–V measurement

Fig. 1 shows the typical DLTS results for $In_{0.78}Ga_{0.22}As$/InP detectors. One broad deep trap signal is detected under forward filling bias, concerning to be the minority carrier (hole) trap. Trap energy position is about 0.26 eV, determined from temperature dependence of the thermal emission rates of the traps in the inset picture of Fig. 1. The concentration of this trap is extracted to be $1.4 \times 10^{14}\,cm^{-3}$ by using standard DLTS techniques. The traps in extended wavelength $In_xGa_{1-x}As$ PIN devices have been seldom reported earlier. Some DLTS studies report the deep centers at $E_v + 0.33$ eV,[15] $E_v + 0.37$,[16] $E_v + 0.41$ eV,[17] and $E_v + 0.45$ eV (Ref. 18) in lattice matched $In_{0.53}Ga_{0.47}As$/InP detectors. These defects are widely believed to be related to Fe impurities in $In_{0.53}Ga_{0.47}As$ layers. Small deviation from lattice matched

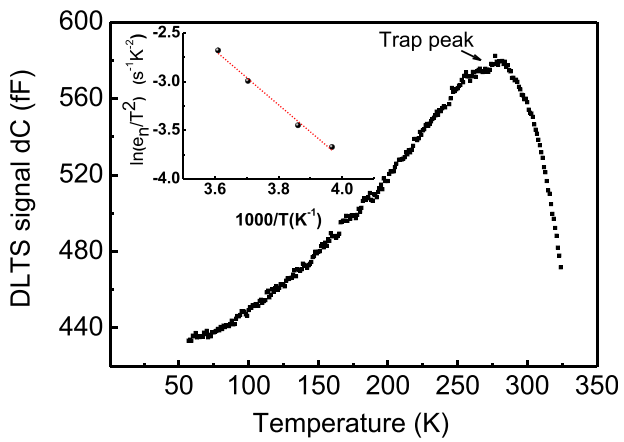

FIG. 1. DLTS spectra for $In_xGa_{1-x}As$/InP detectors with $x = 0.78$ measured at a rate window of $980\,s^{-1}$. The inset shows the Arrhenius plot from which the activation energy for the observed trap is determined.

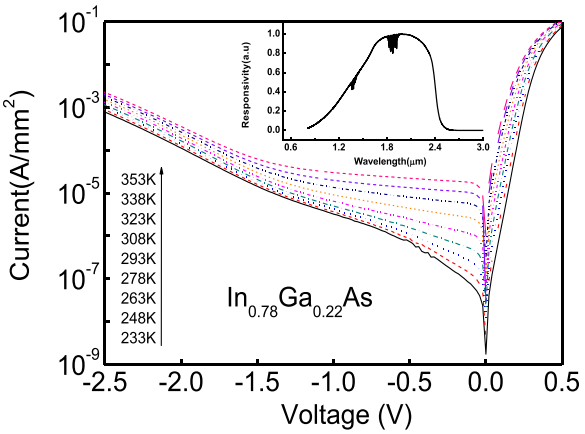

FIG. 2. The temperature dependence of I–V characteristics for $In_xGa_{1-x}As$/InP detectors with $x = 0.78$. The inset shows the relative spectral responsivity at 300 K.

structures causes two new deep centers with energy level at $E_C - 0.1$ eV and $E_C - 0.48$ eV on dislocation or defect scenario.[15,19] As the deep level trap detected here exhibits the rather high concentration, it is hard to believe the impurities can be present at such concentration. It is considered that the trap revealed by DLTS measurements is associated with the dislocation due to the lattice mismatch in $In_{0.78}Ga_{0.22}As$ layer. The activation energy of the deep trap is near the half of the energy band gap of $In_{0.78}Ga_{0.22}As$ material ($E_g = 0.52$ eV) and the concentration levels of this electrically active defects are high enough to have a deleterious effect on the electrical performance of the detectors.

Figure 2 shows typical I–V curves of $In_{0.78}Ga_{0.22}As$ photo-detector at the various temperatures. The inset shows the relative spectral responsivity at 300 K, informing that the response wavelength range of the detectors is between 1 μm and 2.4 μm. The voltage and temperature behaviors in the high and low bias voltage ranges are different. In the high reverse voltage range with V_R higher than -1.5 V, the dark current exhibits exponential increases with the applied voltage. The strong bias dependence could be associated with the field enhancement leakage process as band-to-band tunneling (BBT). This suggestion is supported by the weak

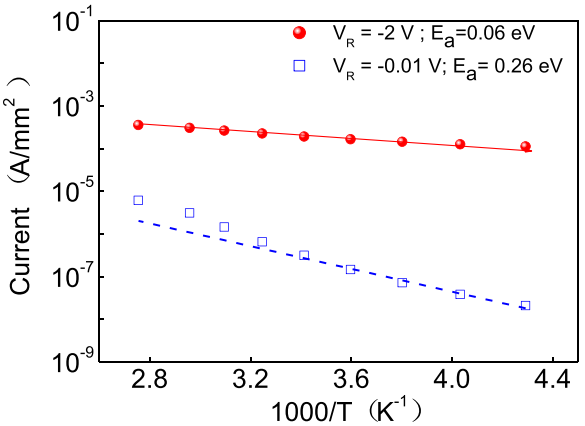

FIG. 3. Dark current versus 1000/T at the reverse bias voltage $V_R = -2$ V and $V_R = -0.01$ V.

thermal dependence of current in this voltage range. As shown in Fig. 3, the activation energy E_a at $V_R = -2$ V is about 0.06 eV. Nearly athermal behavior confirms the dark current in the high reverse bias range can be described by BBT mechanism.[20] On the other hand, in the low bias range with V_R below −1.5 V, the temperature patterns changes. A relative strong temperature dependent dark current is observed, for example, the deduced temperature activation energy E_a at $V_R = -0.01$ V is about 0.26 eV, seen in Fig. 3. As this activation energy values are near the half of the energy band gap of $In_{0.78}Ga_{0.22}As$ material ($E_g = 0.52$), the dark current in the low reverse bias range is expected from a Shockley-Hall-Read (SRH) generation mechanism. However, the conventional SRH current exhibits square root dependence with the applied voltage, which is inadequate to explain the strong voltage dependence of dark current observed in the temperature range lower than 263 K in the low negative voltage range.

B. Dark current models

To understand the dark current mechanism of $In_{0.78}Ga_{0.22}As/InP$ detectors in the measured temperature and voltage range, the device simulation is carried out by Silvaco Altas.[21] The structure used for the simulation is shown in Fig. 4(a), which includes a 0.5 μm heavily p-doped $InAs_{0.53}P_{0.47}$ cap layer with doping density of 4×10^{18} cm^{-3}, a 4.5 μm unintentionally doped $In_{0.78}Ga_{0.22}As$ absorbing layer with electron density of 7×10^{16} cm^{-3}, 1 μm heavily n-doped $InAs_xP_{1-x}$ (x = 0∼0.53) buffer layer with doping density of 6×10^{18} cm^{-3}, and a InP substrate with doping density of 1×10^{16} cm^{-3}.

Usually, the dark current of PIN photo-detectors is modeled by three distinct mechanisms: diffusion, SRH generation, and BBT. As we mentioned above, SRH generation mechanism is inadequate to explain the experimental results in the low reverse voltage. On the other hand, under the presence of deep trap levels, trap-assisted tunneling could occur. Therefore, trap assisted tunneling (TAT) mechanism is considered in the dark current model. The total dark current can be expressed as

$$I_{TOTAL} = I_{DIFF} + I_{BBT} + I_{SRH} + I_{TAT}. \quad (1)$$

In Silvaco Altas,[21] the tunneling generation rate G_{BBT} for BBT current is described as

$$G_{BTBT} = AE^{\gamma} \exp\left(-\frac{B}{E}\right). \quad (2)$$

Here, E is the magnitude of the electric field, A, γ and B are definable parameters that can be altered in order to better characterize the curves. As the parameter γ of BBT is usually equal 2 for narrow band IR detectors,[21–23] γ value is fixed to 2 in the simulation. For SRH generation, the net generation rate of electrons is defined as

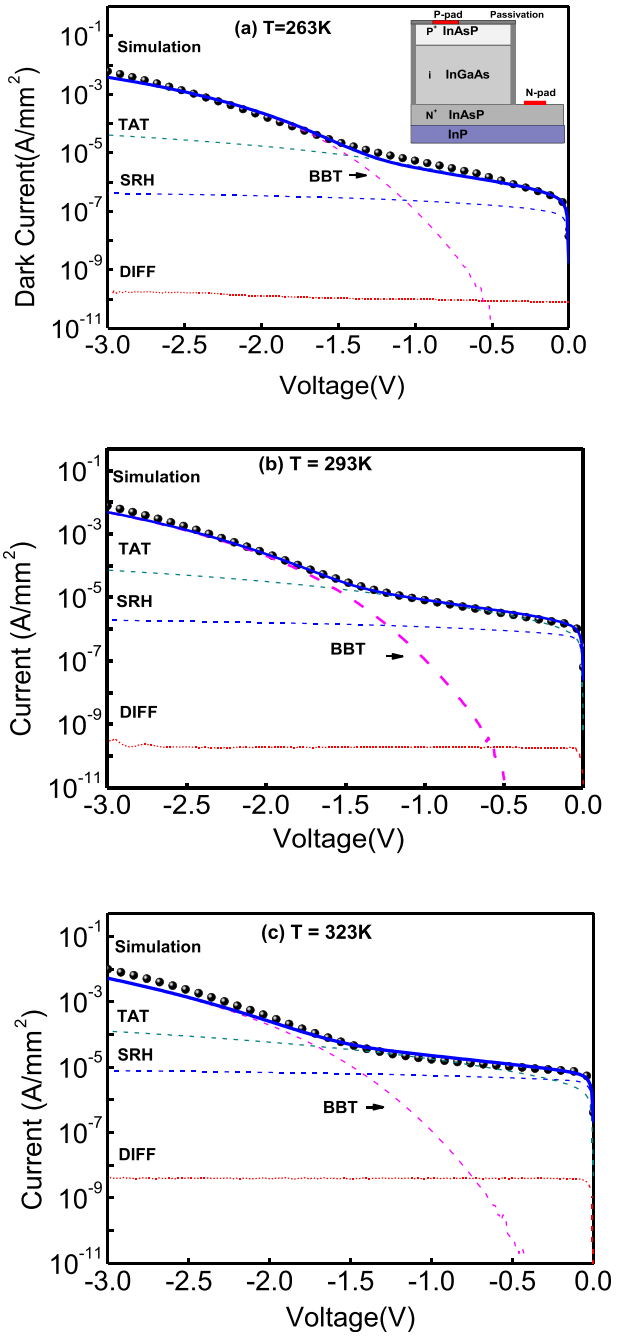

FIG. 4. The experimental and simulated I–V curves at three different temperatures (a) T = 263 K, the inset shows the schematic of the device; (b) T = 293 K and (c) T = 323 K. The solid circles in the plots present the measured data while the solid and the dash lines are the simulated results and their four components, respectively. It is seen that TAT and SRH currents are the major contributors for the dark current at the low bias voltage.

$$R_{SRH} = \frac{N_T(pn - n_i^2)}{\tau_{p0}\left[n + n_i \exp\left(\frac{E_i - E_T}{kT}\right)\right] + \tau_{n0}\left[p + n_i \exp\left(\frac{E_T - E_i}{kT}\right)\right]}, \quad (3)$$

where τ_{p0} and τ_{n0} are the electron and hole lifetimes due to SRH processes, n_i and E_i are the intrinsic carrier concentration and intrinsic Fermi level; E_T and N_T are the trap level and trap concentrations, n and p are the electron and hole concentrations, respectively; The symmetric behaviors occur for holes.

For dark current due to TAT process, the generation rate due to tunneling is calculated by including appropriate field enhancement factors (Γ_p^{DIRAC} and Γ_n^{DIRAC}) in the carrier lifetimes in Eq. (3). These enhancement factors include the effects of field-assisted tunneling on the emission of electrons and holes from a trap. The generation rate of electrons in TAT process[21] is given as

$$R_{TAT} = \frac{N_T(pn - n_{ie}^2)}{\frac{\tau_{p0}}{1+\Gamma_p^{DIRAC}}\left[n + n_i \exp\left(\frac{E_i - E_T}{kT}\right)\right] + \frac{\tau_{n0}}{1+\Gamma_n^{DIRAC}}\left[p + n_i \exp\left(\frac{E_T - E_i}{kT}\right)\right]}. \quad (4)$$

Here, the terms Γ_n^{DIRAC} and Γ_p^{DIRAC} are given by

$$\Gamma_{n,p}^{DIRAC} = \frac{\Delta E_{n,p}}{kT}\int_0^1 \exp\left(\frac{\Delta E_{n,p}}{kT}\left(u - K_{n,p}u^{\frac{3}{2}}\right)\right)du, \quad (5)$$

where u is the integration variable, $\Delta E_{n,p}$ is the energy range where tunneling can occur for electrons or holes, and $K_{n,p}$ is defined as

$$K_{n,p} = \frac{4}{3}\frac{\sqrt{2m_0 m_{traps}(\Delta E_{n,p})^3}}{3qh|E|}. \quad (6)$$

Here, $|E|$ is the absolute value of the electric field, m_{traps} is the effective mass used for carrier tunneling.

TAT mechanism is used to reproduce the tunneling current assisted by the specific traps. Under the higher electric fields, the tunneling carriers may bridge the forbidden gap directly and give rise to band to band tunneling currents. As the thermal emission gives rise of a temperature dependence of the TAT generation rate in Eq. (4), the temperature dependence of TAT current is different from that of BBT current.

C. Deep-level traps induced dark currents

In the devices simulation, the trap revealed by DLTS measurements is considered as SRH generation site and TAT trap center. Fig. 4 shows the simulated and experimental reverse I–V curves of $In_{0.78}Ga_{0.22}As$ detectors at 263 K, 293 K, and 323 K. The solid circles are the measured data points while the solid and dashed lines present the total simulation current and their four components, respectively. For the current component such as (SRH, BBT, TAT), it cannot be determined individually by Silvaco-Altas. Instead, (SRH+DIFF) current could be calculated by the software. SRH component is then obtained from the difference between (SRH+DIFF) and DIFF. Other components are also obtained in the similar way. The parameters used in the simulation are listed in Table I. Values for the physical parameters such as intrinsic carrier concentration, electron and hole mobility, carrier lifetimes, diffusion lengths, and dielectric constant in respective regions have been taken according to standard data for $In_xGa_{1-x}As$ materials implanted in Silvaco Altas.

The proposed model demonstrates a closer fit to the experimental I–V characteristics at various temperatures. It is seen that under the high reverse biases with V_R higher than −1.5 V, the dark current is dominated by BBT mechanism which is in favor of validity of the previous analysis. On the other hand, the dark current in the low bias voltage range exhibits complicate mechanisms. Table II shows the dark current constituents at a fixed voltage $V_R = -0.01$ V for five different temperatures. It is found that deep-level trap induced SRH and TAT currents are the major sources for the dark current flowing in the detectors near the room temperature (T = 293 K). However, the contribution factor of the two components is strongly dependent with the temperature. At the room temperature (293 K), SRH and TAT are almost equal to each other and both are the dominate contributors for the dark current. Lowering

TABLE I. The parameters used in the simulation for $In_{0.78}Ga_{0.22}As$ /InP detectors.

Parameter nomenclature unit		Value
In composition	x	0.78
Band gap	E_g (eV)	0.52
Trap energy level	E_T (eV)	$E_v + 0.26$
Trap concentration	N_T (cm^{-3})	1.4×10^{14}
Electron capture cross section	σ_n (cm^2)	6×10^{-16}
Hole capture cross section	σ_p (cm^2)	2×10^{-15}
BBT parameters	A	1.9×10^{19}
BBT parameters	B (vm^{-1})	3.3×10^6
BBT parameters	γ	2
TAT effective mass	m_{traps}	0.03

TABLE II. The dark current constitutions under the low reverse bias $V_R = -0.01$ (V) at various temperatures.

(A/mm^2)	233 K	263 K	293 K	323 K	353 K
I_{DIFF}	6.5×10^{-11}	7.9×10^{-11}	5.0×10^{-11}	1.1×10^{-9}	1.5×10^{-8}
I_{TAT}	1.2×10^{-8}	7.3×10^{-8}	1.6×10^{-7}	4.1×10^{-7}	9.4×10^{-7}
I_{SRH}	2.8×10^{-9}	2.5×10^{-8}	1.9×10^{-7}	1.2×10^{-6}	5.8×10^{-6}
I_{TOTAL}	1.4×10^{-8}	7.6×10^{-8}	3.4×10^{-7}	1.6×10^{-6}	6.8×10^{-6}

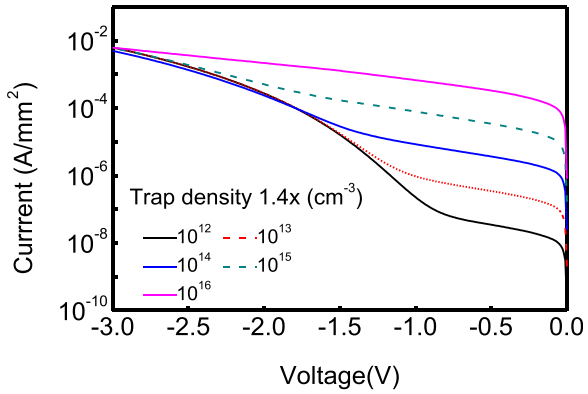

FIG. 5. The influence of the deep level traps density on the room temperature dark current. The density is varied from 1.4×10^{16} to 1.4×10^{12} cm^{-3} in steps of one order.

temperature down from 293 K seems to reduce SRH current dramatically, i.e., from 1.9×10^{-7} (A/mm^2) at 293 K to 2.8×10^{-9} (A/mm^2) at 233 K. However, TAT current shows relatively weak temperature dependence due to the quantum effect. At the temperature of 233 K, TAT current is about 5 times larger than SRH current and becomes the major contributor for dark currents. It is predicted that further reducing the temperature could strongly suppress SRH but can not reduce TAT current largely. It is noteworthy also that the diffusion currents show a values lower than 10^{-11} A/mm^2 even at the room temperature, which is five order smaller than SRH and TAT currents. Therefore, the diffusion current in the detectors can be neglected. The weak diffusion process is proposed to be due to the significant band barriers and the band discontinuities in the space-charge regions of $InAs_yP_{1-y}$ and $In_xGa_{1-x}As$ hetero-structure.[24]

The deep level traps characteristic determine SRH and TAT currents. To further identify the importance of the traps, we study the influence of the traps density on the dark current at room temperature. Fig. 5 shows the simulated I–V curves by changing the trap concentration from 1.4×10^{16} cm^{-3} to 1.4×10^{12} cm^{-3} in steps of one order; here the trap level is fixed to the values from DLTS measurements. It can be seen that the deep traps density strongly modify the behavior of the dark current at the low bias voltage region. Per order decrease of the deep trap density reduces 10 times of the dark current. It is proposed that the "bad" devices with a much higher dark current level are mainly caused by the deep trap induced SRH and TAT currents. Under the results of these tests, it is concluded that further improving the electrical performance of the devices need to improve the material growth and device process to suppress the deep-level traps.

IV. CONCLUSIONS

We have investigated deep-level transient spectroscopy and dark current characteristics of extended wavelength $In_xGa_{1-x}As$ ($x = 0.78$)/InP detectors. The reverse-bias current-voltage characteristics of $In_xGa_{1-x}As$ detectors are simulated by using Shockley-Hall-Read and trap-assisted tunneling mechanisms in conjunction with data from deep-level transient spectroscopy measurement. The results show that deep level trap induced Shockley-Hall-Read and trap-assisted tunneling currents are the major contributors to the dark current in the low reverse bias voltage. The lower trap density benefits for the lower dark currents. These results show that improving the material growth and device process to reduce the deep trap density is a promise choice for the good extended-wavelength InGaAs photo-detectors.

ACKNOWLEDGMENTS

This work was supported by the National Program on Key Basic Research Project (973 Program) of China (Nos. 2010CB934200 and 2012CB619200), the open project of Key Laboratory of Infrared Imaging Materials and Detectors (IIMDKFJJ-12-06), Shanghai Institute of Technical Physics, Chinese Academy of Sciences.

[1]M. MacDougal, J. Geske, C. Wang, and D. Follman, Opt. Eng. **50**, 61011 (2011).
[2]Y. Zhang, Y. Gu, K. Wang, A. Li, and C. Li, Semicond. Sci. Technol. **23**, 125029 (2008).
[3]S. Paul, J. Roy, and P. Basu, J. Appl. Phys. **69**, 827 (1991).
[4]Y. Uchida, H. Kakibayashi, and S. Goto, J. Appl. Phys. **74**, 6720 (1993).
[5]R. Martinelli, T. Zamerowski, and P. Longeway, Appl. Phys. Lett. **53**, 989 (1988).
[6]H. Yuan, G. Apgar, J. Kim, J. Laquindanum, V. Nalavade, P. Beer, J. Kimchi, and T. Wong, Proc. SPIE **6940**, 69403C (2008).
[7]Y. Gu, K. Wang, C. Li, X. Xiang, Y. Cao, and Y. Zhang, J. Infrared Millim. Waves **30**, 481 (2011).
[8]J. Chyi, J. Shieh, J. Pan, and R. Lin, J. Appl. Phys. **79**, 8367 (1996).
[9]Z. Tian, Y. Gu, K. Wang, and Y. Zhang, Chin. Phys. Lett. **25**, 2292 (2008).
[10]C. Li, H. Li, Y. Li, K. Wang, Y. Gu, and Y. Zhang, Semicond. Optoelectron. **30**, 6 (2009).
[11]G. Miao, T. Zhang, Z. Zhang, and Y. Jin, CrystEngComm **15**, 8461 (2013).
[12]R. Hoogeveen, R. vander, and A. Goede, Infrared Phys. Technol. **42**, 1 (2001).
[13]W. Loke, S. Yoon, S. Wicaksono, K. Tan, and K. Lew, J. Appl. Phys. **102**, 054501 (2007).
[14]O. Yastrubchak, T. Wosinski, A. Makosa, T. Figielski, and A. Toth, Physica B **308–310**, 757 (2001).
[15]A. Kowalczyk, L. Ornoch, J. Muszalski, J. Kaniewski, and J. Bak-Misiuk, Optica. Applicata. **35**, 457 (2005).
[16]Z. Chen, T. Wolf, W. Korb, and D. Bimberg, J. Appl. Phys. **64**, 4574 (1988).
[17]M. Sugawara, M. Kondo, T. Takanohashi, and K. Nakajima, Appl. Phys. Lett. **51**, 834 (1987).
[18]G. Guillot, G. Bremond, T. Benyattou, F. Ducroquet, B. Wirth, M. Colombet, A. Louati, and A. Bencherifa, Semicond. Sci. Technol. **5**, 391 (1990).
[19]K. Wang and W. Xu, Semicond. Photonics Technol. **1**, 20 (1995).
[20]J. Chang, C. Wu, X. Ji, H. Ma, F. Yan, Y. Shi, and R. Zhang, Chin. Phys. Lett. **29**, 058501 (2012).
[21]*Atlas User's Manual* (SILVACO International, 2007).
[22]W. Hu, X. Chen, Z. Ye, J. Zhang, F. Yin, C. Lin, Z. Li, and W. Lu, J. Electron. Mater. **39**, 981 (2010).
[23]W. Hu, X. Chen, F. Yin, Z. Quan, Z. Ye, X. Hu, Z. Li, and W. Lu, J. Appl. Phys. **105**, 104502 (2009).
[24]X. Wang, W. Hua, X. Chena, H. Tang, T. Li, H. Gong, and W. Lu, Opt. Quantum Electron. **40**, 1261 (2008).